

Learning to Learn Weight Generation via Local Consistency Diffusion

Yunchuan Guan^{1,2}, Ke Zhou², Yu Liu², Zhiqi Shen¹, Jenq-Neng Hwang³, and Lei Li^{3,4}

¹Nanyang Technological University

²Huazhong University of Science and Technology

³University of Washington

⁴University of Copenhagen

3 Feb 2025

Abstract

Diffusion-based algorithms have emerged as promising techniques for weight generation. However, existing solutions are limited by two challenges: generalizability and local target assignment. The former arises from the inherent lack of cross-task transferability in existing single-level optimization methods, limiting the model’s performance on new tasks. The latter lies in existing research modeling only global optimal weights, neglecting the supervision signals in local target weights. Moreover, naively assigning local target weights causes local-global inconsistency. To address these issues, we propose Mc-Di, which integrates the diffusion algorithm with meta-learning for better generalizability. Furthermore, we extend the vanilla diffusion into a local consistency diffusion algorithm. Our theory and experiments demonstrate that it can learn from local targets while maintaining consistency with the global optima. We validate MC-Di’s superior accuracy and inference efficiency in tasks that require frequent weight updates, including transfer learning, few-shot learning, domain generalization, and large language model adaptation.

1 Introduction

Diffusion-based models have achieved impressive generative performance in various data modalities, ranging from images to structured tabular [15]. Recent works leverage a diffusion model f_ϕ^G to generate neural network weight θ for downstream tasks [35, 28, 29]. This technology enables training and fine-tuning to be performed in a gradient-free manner, offering promising solutions for tasks that require frequent weight updates. Examples include transfer learning, few-shot learning, domain generalization, and LLM adaptation. However, existing methods are limited by two challenges: generalizability and local target assignment.

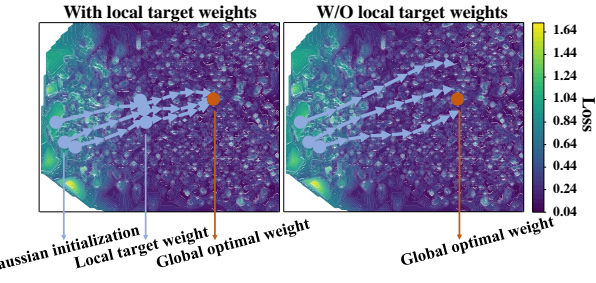


Figure 1: Visualization of inference chains in Omnipigot’s 2D weight-reduced space. Darker areas indicate lower task loss. The model trained with local target weights produces accurate and efficient inference chains.

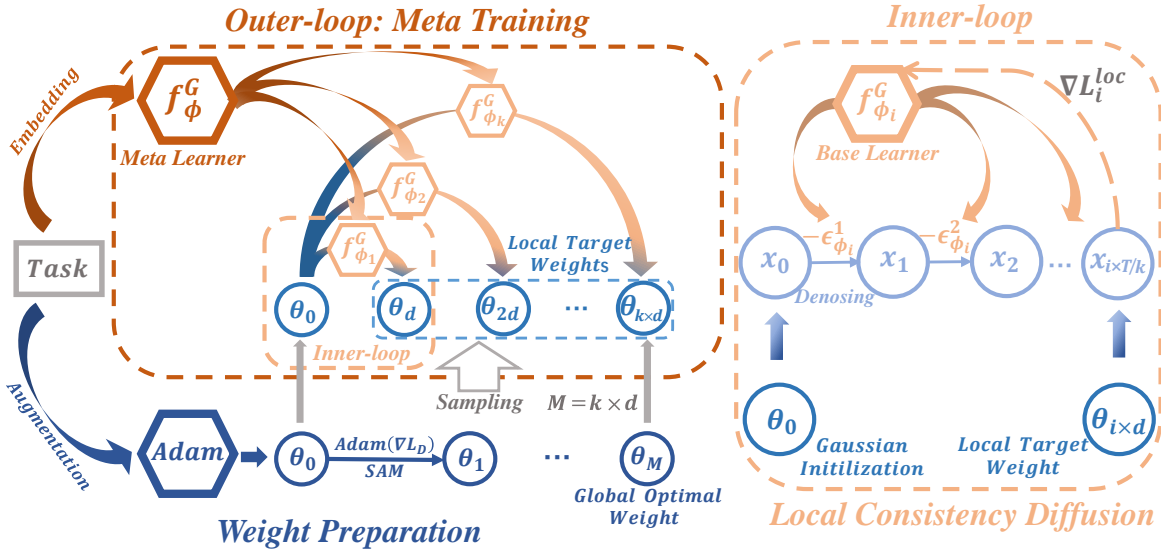


Figure 2: Workflow of Mc-Di. In the weight-preparation stage, a real-world optimizer (Adam) is used to optimize the downstream task. We collect the optimization trajectory, i.e., $\{\theta_i\}_{i=0}^M$, and sample from them to obtain local target weights $\{\theta_{i \times d}\}_{i=1}^k$. In the meta-training stage, a meta-learner f_ϕ^G assigns a base learner $f_{\phi_i}^G$ to each local target weight $\theta_{i \times d}$. Within each inner-loop, the base learner models local targets using local consistency diffusion.

Generalizability. Current studies leverage models such as Variational Autoencoder (VAE) [27] and Hypernetwork [18] to learn the latent distribution of optimal weights for downstream tasks. OCD [35] and D2NWG [47] attempt to use the diffusion model to simulate the weight optimization process. However, these approaches are constrained by single-level optimization frameworks and demonstrate limited capability for knowledge transfer between tasks. This limitation subsequently impacts their generalizability for new tasks [21, 8, 55].

Local target assignment. Existing methods only model global optima θ_M , overlooking the supervision signals in local target weights. These weights are acquired during optimization toward the global optima and contain the policy-specific details of the optimizer. Figure 1 shows that ignoring local targets produces inefficient and low-accuracy inference chains. Moreover, as shown in Figure 3, naively assigning local target weights creates inconsistency between local and global targets. Consequently, assigning local targets while maintaining consistency remains an open and non-trivial challenge.

In this paper, (1) we propose **Meta**-learning weight generation via local **consistency Diffusion**, i.e., Mc-Di. Figure 2 shows Mc-Di’s workflow, which consists of weight preparation and meta-training stages. In the weight preparation stage, local target weights $\{\theta_{i \times d}\}_{i=1}^k$ are collected by sampling the optimization trajectory at uniform intervals of d . In the meta-training stage, we combine bi-level optimization and diffusion algorithms to model local targets for better generalizability. (2) We extend vanilla diffusion to Local Consistency Diffusion. It models local target while maintaining global consistency. Figure 1 shows how local consistency diffusion leverages local targets to guide the inference process. The above characteristics enable Mc-Di to achieve superior generative accuracy and improved inference efficiency. (3) We analyze the convergence properties of the weight generation paradigm and introduce improvements. We decouple functional components, i.e., data augmentation [21] for robustness and Sharpness-Aware Minimization (SAM) [14] for convergence efficiency, from the meta-training stage to the weight preparation stage. This approach improves convergence efficiency without additional time overhead.

Our contributions can be summarized as follows:

- We propose Mc-Di that combines meta-learning and diffusion algorithms for better generalizability.
- We propose local consistency diffusion to model local target weights. It maintains consistency between local and global targets, thus improving generation quality.
- We study the convergence of the weight generation paradigm and introduce SAM to improve efficiency without extra time overhead.

2 Methodology

The proposed Mc-Di consists of two stages: weight preparation and meta-training. It combines bi-level optimization meta-learning with a diffusion algorithm, enabling better generalizability.

2.1 Weight Preparation

As shown below in Figure 2, the weight preparation stage aims to collect and sample local target weights. These weights are acquired during iterations toward the global optima θ_M and contain the policy-specific details of the optimizer, where M represents the downstream training epoch.

Specifically, we use task data T_i and a real-world optimizer, i.e., Adam [26], to optimize the downstream neural network and record the corresponding optimization trajectory $\{\theta_0, \theta_1, \dots, \theta_M\}$. Note that θ_0 is a Gaussian-initialized weight. In our implementation, we uniformly sample from the optimization trajectory. Consequently, the sampled local target weights are $\{\theta_d, \theta_{2d}, \dots, \theta_{k \times d}\}$, where $d = M/k$ and k is the segment number.

Benefiting from the two-stage weight generation paradigm, we can advance functional components from the inner-loop to the weight preparation stage. As shown in Figure 2, we add Sharpness Aware Minimization (SAM) for convergence efficiency and data augmentation for robustness into the weight preparation stage. Meanwhile, since the meta-training stage can start synchronously once a few weights are collected, adding functional components during weight preparation doesn't incur additional time overhead. The specific process of the weight preparation stage is detailed in Algorithm 1.

2.2 Meta-Training

In the meta-training stage, we use a bi-level optimization algorithm, i.e., REPTILE [39], as the framework to ensure efficiency. As shown in the orange region of Figure 2, the meta-learner f_ϕ^G assigns a base learner $f_{\phi_i}^G$ to each local target $\theta_{i \times d}$.¹ Within each inner-loop, the base learner models the generation process of $\theta_0 \rightarrow \theta_{i \times d}$ using local consistency diffusion. To enable learning across multiple tasks and enhance meta-learning, the diffusion model is conditioned on the task embedding Emb_{T_i} , which is calculated by a ResNet101 backbone used by [5]. Considering $\theta_{i \times d}$ as the generation target x_T , a naive inner-loop objective, i.e., vanilla diffusion loss L_i , can be written as

$$L_i = \mathbb{E}_{t \in [0, T]} \|\epsilon_{\phi_i}(x_t, t, Emb_{T_i}) - \epsilon\|^2, \quad (1)$$

$$x_t = \sqrt{\bar{\alpha}_t} \theta_{i \times d} + \sqrt{1 - \bar{\alpha}_t} \epsilon, ,$$

¹The terms “diffusion model”, “meta-learner” f_ϕ^G , and “denoiser” ϵ_ϕ , are used interchangeably in this paper.

Algorithm 1 Weight Preparation

Require: Downstream task weights θ_0 , downstream task loss L^D , perturbation ρ , task distribution \mathcal{T} .

- 1: **for** $T_j \sim \mathcal{T}$ **do**
- 2: **for** t in range(M) **do**
- 3: Add noise and rotated data (i.e., data augmentation)
- 4: $\epsilon \leftarrow \rho \frac{\nabla L^D(T_j; \theta_t)}{\|\nabla L^D(T_j; \theta_t)\|}$ (SAM)
- 5: $\theta_{t+1} \leftarrow \text{Adam}(\theta_t, \nabla_\theta L^D(T_j; \theta_t + \epsilon))$
- 6: Append θ_t in W_j^{of}
- 7: **end for**
- 8: Uniformly sample local target weights $W_j^{loc} = \{\theta_{i \times d}^j\}_{i=1}^k$ from W_j^{of} .
- 9: **end for**
- 10: **Return** $\{W_j^{loc}\}_{j=1}^n$

Algorithm 2 Meta Training (Batch version)

Require: Denoiser weight ϕ , inner-loop step K , learning rate η , meta-learning rate ζ , local target weights set $\{W_j^{loc}\}_{j=1}^n$, meta-batch size B .

- 1: **while** not converged **do**
- 2: **for** repeated B times **do**
- 3: Randomly sample $j \in [0, n], i \in (0, k]$ to determined a local target weight $\theta_{i \times d}^j$
- 4: $\phi_i \leftarrow \phi$
- 5: **for** repeated K times **do**
- 6: $\phi_i \leftarrow \phi_i - \eta \nabla_{\phi_i} L_i^{loc}(\theta_{i \times d}^j, \phi_i)$ (Eq. 2)
- 7: **end for**
- 8: $\Delta_{\phi_i} \leftarrow \phi_i - \phi$
- 9: **end for**
- 10: $\phi \leftarrow \phi + \frac{\zeta}{B} \sum_{i=1}^B \Delta_{\phi_i}$
- 11: **end while**

As shown in Figure 3, vanilla diffusion loss L_i disrupts local-global consistency. In Section 3.1, we propose a local consistency loss L_i^{loc} for this issue, and here we just denote the inner-loop objective by L_i^{loc} .

According to REPTILE, the inner-loop update equation can be written as

$$\phi_i = \phi_i - \eta \nabla_{\phi_i} L_i^{loc},$$

where t is the timestamp, η is the inner-loop learning rate, $\bar{\alpha}_t = \prod_{j=t}^{T-1} \alpha_j$, and $\{\alpha_j\}_{j=0}^T$ is an increasing schedule sequence. Then, the outer-loop process can be written as

$$\phi = \phi + \frac{\zeta}{B} \sum_{i=1}^B (\phi_i - \phi),$$

where ζ is the outer-loop learning rate and B is the meta-batch size. The overall meta-learning process is shown in Algorithm 2. It may raise concerns about computational complexity, as Mc-Di introduces additional local targets for learning. We detail this issue in Section 3.2.1.

2.3 Downstream Task Evaluation

The inference process of Mc-Di aligns with the vanilla diffusion algorithm. It can be written as

$$x_{t+1} = \frac{1}{\sqrt{\bar{\alpha}_{t+1}}} \left(x_t - \sqrt{1 - \bar{\alpha}_{t+1}} \epsilon_\phi(x_t, t) \right). \quad (2)$$

When $i = k$, the local target weight $\theta_{k \times d}$ coincides with the global optimal weight θ_M . This implies that the well-trained diffusion model $f_{\phi^*}^G$ can recover the optimal weight θ_M from Gaussian-initialized weights through iterative inference.²

3 Local Consistency Diffusion and Analysis

In this section, we introduce the proposed local consistency diffusion algorithm and analyze its computational complexity, principle, and convergence.

²We will omit the condition state Emb_{T_i} in the following section for brevity.

3.1 Local Consistency Diffusion

Directly using vanilla diffusion loss in Equation 1 for meta-training creates inconsistency between local and global targets. The top of Figure 3 shows that local targets $\theta_{i \times d}$ and the global optima θ_M are equally treated as the generation target x_T after T denoising steps.³ This naive approach creates inconsistency between local and global targets, leading the introduced local target to negatively affect overall performance. To address this issue, the principle of local consistency diffusion can be described below.

Local consistency diffusion aims to generate a sequence of weights starting from Gaussian noise, where $\theta_d, \theta_{2d}, \dots, \theta_{M=k \times d}$ can be reached at evenly spaced intervals of T/k steps.

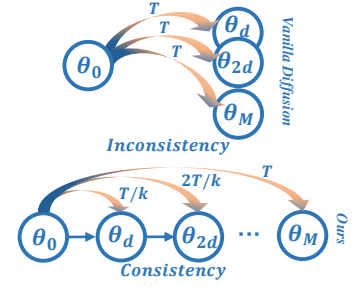


Figure 3: Naively assigning local targets creates inconsistency.

Based on the above principle, we define the local consistency loss L^{loc} below.

Theorem 1. *Given the number of diffusion steps T , an increasing schedule $\{\alpha_0, \dots, \alpha_T\}$, local target weights $\{\theta_d, \dots, \theta_{M=k \times d}\}$, and let the inference process align with the vanilla diffusion algorithm, i.e.,*

$$x_{t+1} = \frac{1}{\sqrt{\bar{\alpha}_{t+1}}} \left(x_t - \sqrt{1 - \bar{\alpha}_{t+1}} \epsilon_\phi(x_t, t) \right).$$

Then, the denoiser ϵ_ϕ can recover the target sequence $\{\theta_d, \dots, \theta_{M=k \times d}\}$ from standard Gaussian noise x_0 with evenly T/k steps intervals, when ϵ_ϕ is trained by local consistency loss L^{loc} as follows:

$$\begin{aligned} L^{loc} &= \underset{i \in (0, k]}{E} L_i^{loc}, \\ L_i^{loc} &= \underset{t \in [0, i \times T/k)}{E} \left\| \sqrt{1 - \bar{\alpha}_t^i} \epsilon_\phi(x_t, t) - \sqrt{1 - \bar{\alpha}_t} \epsilon \right\|^2, \\ x_t &= \sqrt{\bar{\alpha}_t^i} \theta_{i \times d} + \sqrt{1 - \bar{\alpha}_t^i} \epsilon, \end{aligned} \quad (3)$$

where $\bar{\alpha}_t = \prod_{j=t}^{T-1} \alpha_j$, $\bar{\alpha}_t^i = \prod_{j=t}^{i \times T/k - 1} \alpha_j$, and ϵ denotes standard Gaussian noise.

The proof is detailed in Appendix A. In fact, when $k = 1$, local consistency diffusion is equivalent to the vanilla diffusion algorithm. At this point, the denoiser solely models the global optimal weight θ_M . We prove this claim in Appendix B. We refer to the model corresponding to this case as Mv-Di. The right side of Figure 1 depicts the inference chains of Mv-Di. Moreover, existing methods [35, 50, 47] reduce to the $k = 1$ case, so Mc-Di can be regarded as their generalization.

3.2 Analysis

In this section, we discuss issues concerning computational complexity, principles, and convergence.

- How does the segment number k affect computational complexity?
- How does local consistency diffusion enable better efficiency and accuracy?
- The convergence properties of the weight generation paradigm and how to improve them.

³Note that the subscript order of x_t here is reversed compared to the standard diffusion setup. This is to align with the subscript order of the target weights θ_i .

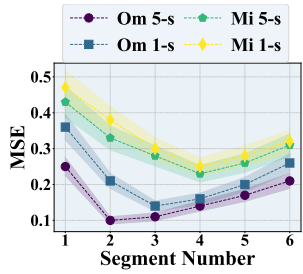


Figure 4: Segment Number vs. MSE trade-off on 5-way 1-shot and 5-shot tasks.

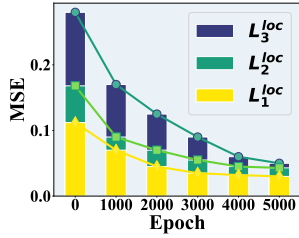


Figure 5: Convergence speed of each L_i^{loc} on Omniglot 5-way 1-shot task.

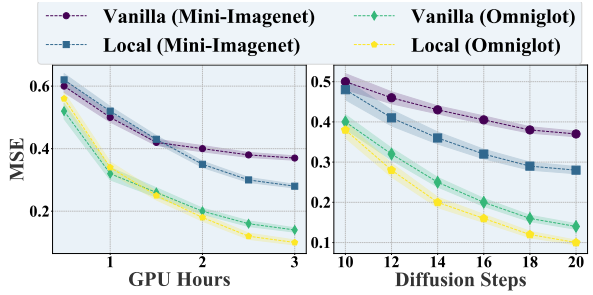


Figure 6: Comparison between vanilla and local consistency diffusion on Mini-ImageNet and Omniglot (5-way 1-shot). Left: GPU hours vs. MSE. Right: Diffusion steps vs. MSE.

3.2.1 Computational complexity

In practice, local consistency diffusion achieves lower computational cost compared to the vanilla diffusion algorithm. This claim contradicts the intuition from Equation 2, where local consistency loss has a computational complexity of $O(k \times T/2)$, compared to $O(T)$ for the vanilla diffusion loss. However, experimental results in Figure 4 and analysis of Figure 5 support our claim.

Under the constraint of three GPU hours, Figure 4 shows the relationship between the segment number k and reconstruction MSE (Mean Square Error) between the final predicted weight and the ground truth weight. We perform a case study on Omniglot [31] and Mini-Imagenet [9] datasets for 5-way tasks. When $k = 1$, our method degenerates into vanilla diffusion. When $k > 1$, our method improves generation accuracy by introducing additional local target $\{\theta_{i \times d}\}_{i=1}^{k-1}$. Note that this result is obtained under the same 3 GPU-hours constraint, highlighting the lower practical computational cost of our method. Considering the stable trade-off across multiple datasets, we set $k = 3$ as the default in subsequent experiments.

3.2.2 Efficiency and Accuracy Improvement

The reduced computational cost of our method can be loosely explained by its division of a search space with radius T into m smaller ones with radius T/k . Figure 5 supports the above claim. When $k = 3$, we record three optimization objectives, i.e., L_1^{loc} , L_2^{loc} , and L_3^{loc} , corresponding to two local target weights $\theta_{M/3}, \theta_{2M/3}$ and a global optimal weight θ_M , on Omniglot 5-way 1-shot tasks. It can be found that L_1^{loc} converges first. This is because $\theta_{M/3}$ is closest to the Gaussian-initialized weight θ_0 and requires the fewest training epochs. Thus, the remaining learning target is to generate θ_M starting from $\theta_{M/3}$. By recursively applying this operation, a T -steps diffusion problem breaks down into k shorter ones. As a result, our method improves practical computational complexity.

Figure 6 compares the trade-off curves between the vanilla diffusion and the local consistency diffusion on Omniglot and Mini-Imagenet 5-way 1-shot tasks. The left figure shows GPU-Hours vs. MSE trade-off, and the right one is Diffusion Steps vs. MSE trade-off. As training progresses, our method increasingly outperforms the vanilla diffusion. The reason is that, in the early stages of training, local consistency diffusion primarily focuses on the learning of prerequisite objectives, such as L_1 and L_2 . Once the learning of these prerequisite objectives is completed, our method converges faster to the optimal weights, i.e., θ_M . Benefiting from this, as shown on the right side of Figure 6, local consistency diffusion can tolerate fewer diffusion steps for the same MSE, thereby enhancing both efficiency and accuracy.

3.2.3 Convergence Analysis and Improvement

The paradigm of learning to generate weights involves two independent loss terms, i.e., downstream task loss L^D and the local consistency loss L^{loc} . This makes ensuring the convergence of the paradigm a non-trivial issue. The following convergence analysis holds for all weight generation methods.

Theorem 2. *Assume that the reconstruction error of the generative model is bounded by c , the downstream loss is bounded by ψ , and the loss function is both l -smooth and μ -strongly convex, with the eigenvalues of the Hessian matrix around the optimum θ_* bounded by λ . Then, the cumulative empirical error of the weight generation paradigm can be bounded as follows:*

$$L^D(\hat{\theta}) - L^D(\theta^*) \leq \frac{\lambda}{2} \left[c + \frac{2\psi}{\mu} \left(1 - \frac{\mu}{l}\right)^M \right], \quad (4)$$

where $\hat{\theta}$ is the weight predicted by the generative model.

The proof, provided in Appendix C, relies on the triangle inequality to decompose the accumulated error into weight preparation error and reconstruction error. Theorem 2 shows that, such a weight generation paradigm affects the overall convergence in only a linear manner, i.e., $c + \frac{2\psi}{\mu} \left(1 - \frac{\mu}{l}\right)^M$. Furthermore, this convergence upper bound can be effectively improved by reducing the maximum eigenvalue λ .

We introduce Sharpness-Aware Minimization (SAM) [14] into the weight preparation stage, to penalize λ by constraining the curvature near global optima. Section 2.1 mentioned that the additional SAM component doesn't incur additional time overhead. Figure 7 shows the effect of SAM on convergence efficiency. The process of SAM is shown in Algorithm 1. Note that although μ -convex is a strong assumption, it does not limit the practicality of our analysis and using SAM. This is because the overall structure of the accumulated error $\lambda(a + b)$ remains unaffected by this assumption.

4 Experiment

Our experimental platform includes two A100 GPUs, one Intel Xeon Gold 6348 processor, and 512 GB of DDR4 memory. For all experiment results, we report the mean and standard deviation over 5 independent repeated experiments. In the following section, we present the basic experimental results and setups, with more details provided in Appendix E.

4.1 Ablation Study

4.1.1 Main Components

The advantages of Mc-Di stem from these main components.

- C1: Combining meta-learning with diffusion-based weight-generation.
- C2: Introducing local target weights to guide the inference chain.
- C3: Using local consistency loss to maintain local-global consistency.

Note that C2 builds on C1, and C3 builds on C2. Therefore, we conduct an incremental ablation study. As shown in Table 1, we validate the effectiveness of each component on Omniglot and

	C1	C2	C3	Omniglot	Mini-Imagenet
REPTILE				95.39 ± 0.09	47.07 ± 0.26
OCD				95.04 ± 0.18	59.76 ± 0.27
Mv-Di	✓			96.65 ± 0.19	62.53 ± 0.37
Tw-Di	✓	✓		94.28 ± 0.31	49.72 ± 0.23
Mc-Di	✓	✓	✓	97.34 ± 0.19	64.87 ± 0.32

Table 1: Ablation of main components on Omniglot and Mini-Imagenet datasets. We record the accuracy of each variant on 5-way 1-shot tasks.

Mini-ImageNet 5-way 1-shot tasks. When none of the components are used, Mc-Di degrades to the REPTILE (meta-learning only) or OCD [35] (diffusion only). When only C1 is used, Mc-Di degrades to Mv-Di. When only using C1 and C2, we refer to this method as Tw-Di.

The comparison between REPTILE and Mv-Di shows the effectiveness of diffusion-based methods. OCD employs a single-layer optimization diffusion, and its comparison with Mv-Di emphasizes the necessity of using meta-learning’s bi-level optimization. When local target weights are introduced without maintaining local-global consistency, Tw-Di underperforms Mv-Di, highlighting the importance of consistency. When introducing local consistency loss, Mc-Di achieves the highest accuracy.

4.1.2 Functional components

Following the setup given by [12], we conducted a case study to evaluate the accuracy improvement and overhead burden brought by each functional component. We incrementally added SAM and data augmentation components to Mc-Di’s data preparation stage. In the Omniglot and Mini-Imagenet datasets, we construct 5-way 1-shot tasks and record the model’s accuracy on the meta-test set at each period of training. Figure 7 shows the GPU Hours vs. Accuracy trade-off curve. The three curves in the figure exhibit identical convergence rates and progressively increasing accuracy. These results demonstrate that adding functional components can improve the model’s performance without additional time overhead at *any stage of training*.

4.2 Comparison Experiments

4.2.1 Transfer Learning

Task. In this task, we train and evaluate models on disjoint pre-training and evaluation datasets. During evaluation, we do not use any labeled data to adjust the models. We evaluated the generalizability of the models using both accuracy and average per-sample evaluation latency.

Dataset. We partitioned ImageNet-1k [7] into 20k subsets of 50 classes each with 50 images per class per task for meta-training. The evaluation datasets are CIFAR-10, CIFAR-100 [30], STL-10 [6], Aircraft [38], and Pets [42].

Baselines. We benchmark against ICIS [5], GHN3 [29], and D2NWG [47]. ICIS directly learns from downstream task samples, while the others learn to generate weights. For all the aforementioned models, the downstream network uses ResNet12 [19] with a linear probe for classification. For the diffusion model f_ϕ^G , Mc-Di employs the same U-Net architecture given by Meta-Diff [50]. The task embedding Emb_{T_i} is calculated by a ResNet101 backbone used by ICIS. In the weight preparation stage, the real-world optimizer (Adam) uses a fixed learning rate of 0.005 and an automatic early-stopping strategy [43] to determine the downstream task training epoch M . In the meta-training

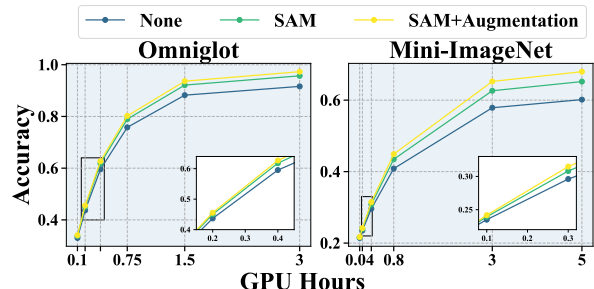


Figure 7: Ablation of functional components. Accuracy vs. GPU Hours trade-off curves on Omniglot 5-way 1-shot tasks.

Method	CIFAR-10	CIFAR-100	STL-10	Aircraft	Pets	Latency (ms)
ICIS [5]	61.75 ± 0.31	47.66 ± 0.24	80.59 ± 0.12	26.42 ± 1.56	28.71 ± 1.60	9.2
GHN3 [29]	51.80 ± 0.42	11.90 ± 0.45	75.37 ± 0.19	23.19 ± 1.38	27.16 ± 1.08	14.5
D2NWG [47]	60.42 ± 0.75	51.50 ± 0.25	82.42 ± 0.04	27.70 ± 3.24	32.17 ± 6.30	6.7
Mv-Di (ours)	61.14 ± 0.32	49.62 ± 0.36	81.43 ± 0.38	29.37 ± 1.22	30.28 ± 1.29	4.7
Mc-Di (ours)	63.57 ± 0.28 $\uparrow 1.82$	50.69 ± 0.49 $\downarrow 0.81$	85.02 ± 0.26 $\uparrow 2.60$	29.97 ± 1.02 $\uparrow 2.27$	35.16 ± 1.18 $\uparrow 2.99$	3.5 $\downarrow \times 1.9$

Table 2: Transfer learning accuracy comparison on various datasets with average per-sample evaluation latency. The gaps indicated by \uparrow and \downarrow represent the difference relative to the second-best method (excluding Mv-Di) on the current task.

Method	Omniglot		Mini-ImageNet		Tiered-ImageNet		Latency (ms)
	(5, 1)	(5, 5)	(5, 1)	(5, 5)	(5, 1)	(5, 5)	
REPTILE [39]	95.39 ± 0.09	98.90 ± 0.10	47.07 ± 0.26	62.74 ± 0.37	49.12 ± 0.43	65.99 ± 0.42	20.7
Meta-Baseline [4]	97.75 ± 0.25	99.68 ± 0.18	58.10 ± 0.31	74.50 ± 0.29	68.62 ± 0.29	83.29 ± 0.51	19.4
Meta-Hypernetwork [53]	96.57 ± 0.22	98.83 ± 0.16	52.50 ± 0.28	67.76 ± 0.34	53.80 ± 0.35	69.98 ± 0.42	13.1
GHN3 [29]	95.23 ± 0.23	98.65 ± 0.19	63.22 ± 0.29	76.79 ± 0.33	64.72 ± 0.36	78.40 ± 0.46	17.5
OCD [35]	95.04 ± 0.18	98.74 ± 0.14	59.76 ± 0.27	75.16 ± 0.35	60.01 ± 0.38	76.33 ± 0.47	8.4
Meta-Diff [50]	94.65 ± 0.65	97.91 ± 0.53	55.06 ± 0.81	73.18 ± 0.64	57.77 ± 0.90	75.46 ± 0.69	8.9
D2NWG [47]	96.77 ± 6.13	98.94 ± 7.49	61.13 ± 8.50	76.94 ± 6.04	65.33 ± 6.50	85.05 ± 8.25	10.4
Mv-Di (ours)	96.65 ± 0.19	99.34 ± 0.23	62.53 ± 0.37	76.25 ± 0.28	64.72 ± 0.17	83.26 ± 0.49	6.4
Mc-Di (ours)	97.34 ± 0.19 $\downarrow 0.41$	99.14 ± 0.13 $\downarrow 0.54$	64.87 ± 0.32 $\uparrow 1.65$	79.98 ± 0.18 $\uparrow 3.04$	70.45 ± 0.27 $\uparrow 1.83$	88.58 ± 0.21 $\uparrow 3.53$	4.8 $\downarrow \times 1.8$

Table 3: Few-shot task accuracy comparison on Omniglot, Mini-ImageNet, and Tiered-ImageNet datasets with average per-sample evaluation latency.

stage, we set the learning rate η , meta-learning rate ζ , inner-steps, and training epochs to 0.005, 0.001, 3, and 6000, respectively. The segment number k is set to 3, and the diffusion step T is set to 20. **We maintain this setup across all experiments in this paper.**

Results. Table 2 shows that Mc-Di achieves the highest accuracy on five out of six tasks while reducing average latency. Compared to the second-best method (except for Mv-Di) on each task, it yields an average accuracy improvement of 2.42%. On CIFAR-100, its accuracy is only 0.81% lower than the best-performing method. Compared to the fastest existing method (i.e., D2NWG), Mc-Di reduces inference latency by $1.9\times$. As discussed in Section 4.1, Mc-Di also outperforms its simplified variant Mv-Di, demonstrating the effectiveness of introducing local target weights.

4.2.2 Few-Shot Learning

Task. Following the setup provided by [12], we train and evaluate models on disjoint meta-training and meta-testing tasks. During the evaluation stage, we use the support set in meta-test tasks to fine-tune the models, and then measure the accuracy and average per-sample evaluation latency on the query set.

Dataset. We use Omniglot [31], Mini-ImageNet [9], and Tiered-ImageNet [45] datasets for the construction of 5-way 1-shot, 5-way 5-shot tasks. To evaluate generalization capabilities, we maintain distinct and separate class sets for training and evaluation phases.

Baselines. Our benchmarks consist of gradient-based methods, including REPTILE [39] and Meta-Baseline [4], and weight generation-based methods, including Meta-Hypernetwork [53], GHN3 [29], OCD [35], Meta-Diff [50], and D2NWG [47]. Following the setting given by MAML [12], the downstream neural network uses four convolution blocks with a linear probe for classification.

Results. Table 2 shows that Mc-Di can improve performance on almost all tasks. Since the 5-way task of Omniglot is relatively easy to learn, the gradient-based method Meta-Baseline can achieve slightly higher accuracy. On the winning tasks, compared to the second-best method, Mc-Di achieves an average improvement of 2.51% in accuracy. Compared to the current fastest weight generation algorithm, i.e., OCD, Mc-Di achieves a $1.8\times$ reduction in inference latency. Note that the gradient-based methods, REPTILE and Meta-Baseline, exhibit high latency here due to the need for gradient computation during fine-tuning.

Method	DomainNet			MRPC			QNLI	
	(5, 1)	(20, 5)	Latency (ms)	Method	Acc	Latency (h)	Acc	Latency (h)
REPTILE [39]	48.13 \pm 0.50	52.32 \pm 0.42	26.8	Full-fine-tune	90.24 \pm 0.57	1.47	92.84 \pm 0.26	3.15
Meta-Baseline [4]	50.54 \pm 0.47	54.45 \pm 0.40	26.2	LoRA [22]	89.76 \pm 0.69	0.81	93.32 \pm 0.20	1.76
Meta-Hypernetwork [53]	59.00 \pm 0.39	63.32 \pm 0.35	10.3	AdaLoRA [52]	88.71 \pm 0.73	0.74	93.17 \pm 0.25	1.68
OCD [35]	64.58 \pm 0.42	67.10 \pm 0.38	9.7	DyLoRA [54]	89.59 \pm 0.81	0.76	92.21 \pm 0.32	1.63
GHN3 [29]	63.11 \pm 0.36	66.42 \pm 0.33	30.1	FourierFT [36]	90.03 \pm 0.54	0.68	92.25 \pm 0.15	1.55
Meta-Diff [50]	64.24 \pm 0.41	67.58 \pm 0.39	10.9	Mv-Di (ours)	88.73 \pm 0.64	0.22	91.04 \pm 0.23	0.48
Mv-Di (ours)	67.04 \pm 0.29	70.15 \pm 0.41	7.5	Mc-Di (ours)	89.43 \pm 0.70	\downarrow 0.60	0.19 \downarrow 3.6	91.86 \pm 0.29
Mc-Di (ours)	69.05 \pm 0.39 \uparrow 4.47	72.86 \pm 0.31 \uparrow 5.28	5.8 \downarrow 1.7	Mc-Di (ours)	89.43 \pm 0.70	\downarrow 0.60	0.19 \downarrow 3.6	91.86 \pm 0.29 \downarrow 1.31 0.41 \downarrow 4.0

Table 4: Accuracy and average per-sample evaluation latency on DomainNet 5-way 1-shot and 20-way 5-shot task.

Table 5: Accuracy and fine-tuning latency comparison on MRPC and QNLI tasks for different fine-tuning algorithms.

4.2.3 Domain Generalization

Task. In this task, we explore the domain generalizability of Mc-Di. We follow the domain generalization few-shot task given by [17] to evaluate the model’s performance.

Dataset. We use DomainNet [32] for the construction of 5-way 1-shot and 20-way 5-shot tasks. Specifically, we use Clipart, Infograph, Painting, Quickdraw, and Real domains for meta-training, while Sketch domains for meta-testing. Under this setting, the tasks in the meta-training set may come from different domains, and the tasks in the meta-testing set may come from another unseen domain.

Baselines. We benchmark against REPTILE, Meta-baseline, Meta-Hypernetwork, GHN3, OCD, Meta-Diff, and D2NWG. The downstream network uses ResNet12 with a linear probe for classification.

Results. Table 4 shows that Mc-Di significantly outperforms current methods on few-shot domain generalization tasks. Compared to the second-best baselines in each task, Mc-Di achieved an average improvement of 4.64% in accuracy. It can be observed that Mc-Di achieves a significant performance improvement over other methods, owing to its integration of meta-learning with weight generation and its maintenance of local-global consistency. In terms of overhead, Mc-Di achieves a 1.7 \times reduction in latency compared to OCD, showing the same advantage as in transfer learning and few-shot learning tasks.

4.2.4 Large Language Model fine-tuning

Task. We demonstrate that Mc-Di can be applied to the fine-tuning of Large Language Models by learning to generate LoRA [22] matrices for new tasks. We compared the algorithms in terms of their fine-tuning accuracy upon convergence and the latency required to achieve it.

Datasets. We conduct a case study to demonstrate the generalizability and efficiency of Mc-Di. We use five binary classification tasks, i.e., SST-2, QQP, RTE, WNLI, and CoLA from the GLUE [49] benchmark for pre-training. Then we use the other two tasks, i.e., MRPC and QNLI, to evaluate the performance of the methods.

Baselines. We benchmark against Full-fine-tuning baseline, LoRA [22], AdaLoRA [52], DyLoRA [54], and FourierFT [36], which are all gradient-based fine-tuning algorithms. The large language model we fine-tuned is RoBERTa-base [36]. The LoRA matrices are generated following the fine-tuning process given by [36]. Note that Mc-Di is a meta-learning-based method that can learn on all training tasks, while other baselines are single-task fine-tuning methods that only work on one task. Note that Mc-Di requires extra time to pre-train the diffusion model f_ϕ^G ; however, this is a one-time cost and demonstrates better potential in multi-task fine-tuning scenarios.

Results. Table 5 shows that Mc-Di achieves comparable binary classification accuracy on two evaluation tasks compared to other gradient-based fine-tuning algorithms while significantly accel-

erating the fine-tuning speed by $\times 3.6$ to $\times 4.0$. By incorporating meta-learning, Mc-Di efficiently captures shared representations from pre-training tasks, enabling the direct, gradient-free generation of task-specific LoRA matrices.

5 Conclusion and Limitation

Conclusion. In this paper, we propose Mc-Di, which integrates the fast inference ability of weight generation technology and the cross-task transferability of bi-level optimization. Building on this, we further propose local consistency diffusion, enabling the model to capture optimization policy in local target weights. It employs a step-by-step approach to assign local targets, elegantly preserving consistency with the global optima. In addition, we theoretically and empirically demonstrate that the convergence of the weight generation paradigm can be improved by introducing SAM. We validate Mc-Di’s superior accuracy and inference efficiency in tasks that require frequent weight updates, such as transfer learning, few-shot learning, domain generalization, and large language model adaptation.

Limitation and future work. Our method builds on the existing diffusion-based weight generation framework. Diffusion models typically depend on a fixed inference starting point—namely, Gaussian noise—which limits the model’s ability to capture local supervisory signals. As shown in Figure 3, a more intuitive way to improve weight generation is to learn arbitrary sub-trajectories $\theta_i \rightarrow \theta_j$ rather than fix trajectories $\theta_0 \rightarrow \theta_j$. In future work, we will adopt more general techniques, such as Flow Matching [33] and Trajectory Balance [1, 51, 41, 37, 23], to model the weight generation problem and break through this limitation.

References

- [1] Yoshua Bengio et al. Flow network based generative models for non-iterative diverse candidate generation. In *Advances in Neural Information Processing Systems 34 (NeurIPS 2021)*, 2021.
- [2] Jiaxin Chen, Xiao-Ming Wu, Yanke Li, Qimai Li, Li-Ming Zhan, and Fu-Lai Chung. A closer look at the training strategy for modern meta-learning. In Hugo Larochelle, Marc'Aurelio Ranzato, Raia Hadsell, Maria-Florina Balcan, and Hsuan-Tien Lin, editors, *Advances in Neural Information Processing Systems 33: Annual Conference on Neural Information Processing Systems 2020, NeurIPS 2020, December 6-12, 2020, virtual*, 2020.
- [3] Qi Chen, Changjian Shui, and Mario Marchand. Generalization bounds for meta-learning: An information-theoretic analysis. In Marc'Aurelio Ranzato, Alina Beygelzimer, Yann N. Dauphin, Percy Liang, and Jennifer Wortman Vaughan, editors, *Advances in Neural Information Processing Systems 34: Annual Conference on Neural Information Processing Systems 2021, NeurIPS 2021, December 6-14, 2021, virtual*, pages 25878–25890, 2021.
- [4] Yinbo Chen, Zhuang Liu, Huijuan Xu, Trevor Darrell, and Xiaolong Wang. Meta-baseline: Exploring simple meta-learning for few-shot learning. In *2021 IEEE/CVF International Conference on Computer Vision, ICCV 2021, Montreal, QC, Canada, October 10-17, 2021*, pages 9042–9051. IEEE, 2021.
- [5] Anders Christensen, Massimiliano Mancini, A. Sophia Koepke, Ole Winther, and Zeynep Akata. Image-free classifier injection for zero-shot classification. In *IEEE/CVF International Conference on Computer Vision, ICCV 2023, Paris, France, October 1-6, 2023*, pages 19026–19035. IEEE, 2023.
- [6] Adam Coates, Andrew Y Ng, and Honglak Lee. An analysis of single-layer networks in unsupervised feature learning. In *Proceedings of the 14th International Conference on Artificial Intelligence and Statistics (AISTATS)*, pages 215–223, 2011.
- [7] Jia Deng, Wei Dong, Richard Socher, Li-Jia Li, Kai Li, and Li Fei-Fei. Imagenet: A large-scale hierarchical image database. In *Proceedings of the IEEE Conference on Computer Vision and Pattern Recognition (CVPR)*, pages 248–255. IEEE, 2009.
- [8] Meng Ding, Mingxi Lei, Yunwen Lei, Di Wang, and Jinhui Xu. On stability and generalization of bilevel optimization problems. 2022.
- [9] Jeff Donahue, Yangqing Jia, Oriol Vinyals, Judy Hoffman, Ning Zhang, Eric Tzeng, and Trevor Darrell. Decaf: A deep convolutional activation feature for generic visual recognition. In *Proceedings of the 31th International Conference on Machine Learning, ICML 2014, Beijing, China, 21-26 June 2014*, volume 32, pages 647–655. JMLR.org, 2014.
- [10] Yingjun Du, Zehao Xiao, Shengcai Liao, and Cees G. M. Snoek. Protodiff: Learning to learn prototypical networks by task-guided diffusion. In *Advances in Neural Information Processing Systems 36 (NeurIPS 2023)*, 2023.
- [11] Alireza Fallah, Aryan Mokhtari, and Asuman E. Ozdaglar. On the convergence theory of gradient-based model-agnostic meta-learning algorithms. In Silvia Chiappa and Roberto Calandra, editors, *The 23rd International Conference on Artificial Intelligence and Statistics, AISTATS 2020, 26-28 August 2020, Online [Palermo, Sicily, Italy]*, volume 108 of *Proceedings of Machine Learning Research*, pages 1082–1092. PMLR, 2020.

[12] Chelsea Finn, Pieter Abbeel, and Sergey Levine. Model-agnostic meta-learning for fast adaptation of deep networks. In *Proceedings of the 34th International Conference on Machine Learning, ICML 2017, Sydney, NSW, Australia, 6-11 August 2017*, volume 70, pages 1126–1135. PMLR, 2017.

[13] Sebastian Flennerhag, Yannick Schroecker, Tom Zahavy, Hado van Hasselt, David Silver, and Satinder Singh. Bootstrapped meta-learning. In *The Tenth International Conference on Learning Representations, ICLR 2022, Virtual Event, April 25-29, 2022*. OpenReview.net, 2022.

[14] Pierre Foret, Ariel Kleiner, Hossein Mobahi, and Behnam Neyshabur. Sharpness-aware minimization for efficiently improving generalization. In *Proceedings of the International Conference on Learning Representations (ICLR)*, 2022.

[15] Roberto Gozalo-Brizuela and Eduardo C. Garrido-Merchán. A survey of generative AI applications. *CoRR*, abs/2306.02781, 2023.

[16] Jiechao Guan and Zhiwu Lu. Task relatedness-based generalization bounds for meta learning. In *The Tenth International Conference on Learning Representations, ICLR 2022, Virtual Event, April 25-29, 2022*. OpenReview.net, 2022.

[17] Yunchuan Guan, Yu Liu, Ke Zhou, and Junyuan Huang. Hierarchical meta-learning with hyper-tasks for few-shot learning. In *Proceedings of the 32nd ACM International Conference on Information and Knowledge Management, CIKM 2023, Birmingham, United Kingdom, October 21-25, 2023*, pages 587–596. ACM, 2023.

[18] David Ha, Andrew Dai, and Quoc V. Le. Hypernetworks. In *International Conference on Learning Representations (ICLR)*, 2017.

[19] Kaiming He, Xiangyu Zhang, Shaoqing Ren, and Jian Sun. Deep residual learning for image recognition. In *Proceedings of the IEEE Conference on Computer Vision and Pattern Recognition (CVPR)*, pages 770–778. IEEE, 2016.

[20] Jonathan Ho, Ajay Jain, and Pieter Abbeel. Denoising diffusion probabilistic models. In Hugo Larochelle, Marc’Aurelio Ranzato, Raia Hadsell, Maria-Florina Balcan, and Hsuan-Tien Lin, editors, *Advances in Neural Information Processing Systems 33: Annual Conference on Neural Information Processing Systems 2020, NeurIPS 2020, December 6-12, 2020, virtual*, 2020.

[21] Timothy Hospedales, Antreas Antoniou, Paul Micaelli, and Amos Storkey. Meta-learning in neural networks: A survey. *IEEE transactions on pattern analysis and machine intelligence*, 44(9):5149–5169, 2021.

[22] Edward J. Hu, Yelong Shen, Phillip Wallis, Zeyuan Allen-Zhu, Yuanzhi Li, Shean Wang, and Weizhu Chen. LoRA: Low-rank adaptation of large language models. In *Proceedings of the International Conference on Learning Representations (ICLR)*, 2022.

[23] et al. Jang. Learning energy decompositions for partial inference of gflownets. In *International Conference on Learning Representations (ICLR 2024)*, 2024.

[24] Sharu Theresa Jose and Osvaldo Simeone. An information-theoretic analysis of the impact of task similarity on meta-learning. In *IEEE International Symposium on Information Theory, ISIT 2021, Melbourne, Australia, July 12-20, 2021*, pages 1534–1539. IEEE, 2021.

[25] Sharu Theresa Jose and Osvaldo Simeone. Information-theoretic generalization bounds for meta-learning and applications. *Entropy*, 23(1):126, 2021.

[26] Diederik P Kingma and Jimmy Ba. Adam: A method for stochastic optimization. In *Proceedings of the 3rd International Conference on Learning Representations (ICLR)*, 2015.

[27] Diederik P. Kingma and Max Welling. Auto-encoding variational bayes. In *2nd International Conference on Learning Representations (ICLR)*, 2014. Presented at ICLR 2014 as a conference paper.

[28] Boris Knyazev, Michal Drozdzal, Graham W. Taylor, and Adriana Romero-Soriano. Parameter prediction for unseen deep architectures. In Marc'Aurelio Ranzato, Alina Beygelzimer, Yann N. Dauphin, Percy Liang, and Jennifer Wortman Vaughan, editors, *Advances in Neural Information Processing Systems 34: Annual Conference on Neural Information Processing Systems 2021, NeurIPS 2021, December 6-14, 2021, virtual*, pages 29433–29448, 2021.

[29] Boris Knyazev, Doha Hwang, and Simon Lacoste-Julien. Can we scale transformers to predict parameters of diverse imagenet models? In Andreas Krause, Emma Brunskill, Kyunghyun Cho, Barbara Engelhardt, Sivan Sabato, and Jonathan Scarlett, editors, *International Conference on Machine Learning, ICML 2023, 23-29 July 2023, Honolulu, Hawaii, USA*, volume 202 of *Proceedings of Machine Learning Research*, pages 17243–17259. PMLR, 2023.

[30] Alex Krizhevsky. Learning multiple layers of features from tiny images. Technical report, University of Toronto, 2009.

[31] Brenden M. Lake, Ruslan Salakhutdinov, Jason Gross, and Joshua B. Tenenbaum. One shot learning of simple visual concepts. In *Proceedings of the 33th Annual Meeting of the Cognitive Science Society, CogSci 2011, Boston, Massachusetts, USA, July 20-23, 2011*. cognitivescience-society.org, 2011.

[32] Aristotelis Leventidis, Laura Di Rocco, Wolfgang Gatterbauer, Renée J. Miller, and Mirek Riedewald. Domainnet: Homograph detection for data lake disambiguation. In *Proceedings of the 24th International Conference on Extending Database Technology, EDBT 2021, Nicosia, Cyprus, March 23 - 26, 2021*, pages 13–24. OpenProceedings.org, 2021.

[33] Yaron Lipman, Ricky T. Q. Chen, Heli Ben-Hamu, Maximilian Nickel, and Matt Le. Flow matching for generative modeling. In *International Conference on Learning Representations*, 2023.

[34] Calvin Luo. Understanding diffusion models: A unified perspective. *CoRR*, abs/2208.11970, 2022.

[35] Shahar Lutati and Lior Wolf. OCD: learning to overfit with conditional diffusion models. In Andreas Krause, Emma Brunskill, Kyunghyun Cho, Barbara Engelhardt, Sivan Sabato, and Jonathan Scarlett, editors, *International Conference on Machine Learning, ICML 2023, 23-29 July 2023, Honolulu, Hawaii, USA*, volume 202 of *Proceedings of Machine Learning Research*, pages 23157–23169. PMLR, 2023.

[36] Shikun Ma, Chunyuan Zhou, Saining Xie, Xiangru Chen, Jingjing Liu, and Jianfeng Gao. Fourier frequency tuning for parameter-efficient fine-tuning. In *Proceedings of the IEEE/CVF Conference on Computer Vision and Pattern Recognition (CVPR)*, pages 3456–3467, 2023.

[37] et al. Madan. Learning gflownets from partial episodes for improved convergence and stability. In *Proceedings of the 40th International Conference on Machine Learning (ICML 2023)*, 2023.

[38] Subhransu Maji, Esa Rahtu, Juho Kannala, Matthew Blaschko, and Andrea Vedaldi. Fine-grained visual classification of aircraft. In *arXiv preprint arXiv:1306.5151*, 2013.

[39] Alex Nichol, Joshua Achiam, and John Schulman. On first-order meta-learning algorithms. volume abs/1803.02999, 2018.

[40] Yuval Nirkin, Lior Wolf, and Tal Hassner. Hyperseg: Patch-wise hypernetwork for real-time semantic segmentation. In *IEEE Conference on Computer Vision and Pattern Recognition, CVPR 2021, virtual, June 19-25, 2021*, pages 4061–4070. Computer Vision Foundation / IEEE, 2021.

[41] et al. Pan. Better training of gflownets with local credit and incomplete trajectories. In *Proceedings of the 40th International Conference on Machine Learning (ICML 2023)*, 2023.

[42] Omkar M Parkhi, Andrea Vedaldi, Andrew Zisserman, and CV Jawahar. Cats and dogs. *IEEE Conference on Computer Vision and Pattern Recognition*, 2012.

[43] Lutz Prechelt. Early stopping-but when? In *Neural Networks: Tricks of the trade*, pages 55–69. Springer, 2002.

[44] Aniruddh Raghu, Maithra Raghu, Samy Bengio, and Oriol Vinyals. Rapid learning or feature reuse? towards understanding the effectiveness of MAML. In *8th International Conference on Learning Representations, ICLR 2020, Addis Ababa, Ethiopia, April 26-30, 2020*. OpenReview.net, 2020.

[45] Mengye Ren, Eleni Triantafillou, Sachin Ravi, Jake Snell, Kevin Swersky, Joshua B. Tenenbaum, Hugo Larochelle, and Richard S. Zemel. Meta-learning for semi-supervised few-shot classification. In *International Conference on Learning Representations (ICLR)*, 2018.

[46] Konstantin Schürholt, Boris Knyazev, Xavier Giró-i Nieto, and Damian Borth. Hyper-representations as generative models: Sampling unseen neural network weights. In *Advances in Neural Information Processing Systems (NeurIPS)*, 2022.

[47] Bedionita Soro, Bruno Andreis, Hayeon Lee, Wonyong Jeong, Song Chong, Frank Hutter, and Sung Ju Hwang. Diffusion-based neural network weights generation. *arXiv preprint arXiv:2402.18153*, 2024.

[48] Eleni Triantafillou, Tyler Zhu, Vincent Dumoulin, Pascal Lamblin, Utku Evci, Kelvin Xu, Ross Goroshin, Carles Gelada, Kevin Swersky, Pierre-Antoine Manzagol, and Hugo Larochelle. Meta-dataset: A dataset of datasets for learning to learn from few examples. In *8th International Conference on Learning Representations, ICLR 2020, Addis Ababa, Ethiopia, April 26-30, 2020*. OpenReview.net, 2020.

[49] Alex Wang, Amanpreet Singh, Julian Michael, Felix Hill, Omer Levy, and Samuel R Bowman. Glue: A multi-task benchmark and analysis platform for natural language understanding. *Proceedings of the International Conference on Learning Representations (ICLR)*, 2019.

[50] Baoquan Zhang, Chuyao Luo, Demin Yu, Xutao Li, Huiwei Lin, Yunming Ye, and Bowen Zhang. Metadiff: Meta-learning with conditional diffusion for few-shot learning. In *Thirty-Eighth*

AAAI Conference on Artificial Intelligence, AAAI 2024, Thirty-Sixth Conference on Innovative Applications of Artificial Intelligence, IAAI 2024, Fourteenth Symposium on Educational Advances in Artificial Intelligence, EAAI 2014, February 20-27, 2024, Vancouver, Canada, pages 16687–16695. AAAI Press, 2024.

- [51] et al. Zhang. Unifying generative models with gflownets and beyond. In *Advances in Neural Information Processing Systems 35 (NeurIPS 2022)*, 2022.
- [52] Renrui Zhang, Juntao Li, Yifan Xie, Xun Liu, Yiyang Zhao, Qiang Wang, and Ziwei Liu. AdaLoRA: Towards efficient adaptive low-rank adaptation for large language models. In *Proceedings of the Conference on Neural Information Processing Systems (NeurIPS)*, pages 5678–5689, 2023.
- [53] Dominic Zhao, Seijin Kobayashi, João Sacramento, and Johannes von Oswald. Meta-learning via hypernetworks. In *4th Workshop on Meta-Learning at NeurIPS 2020 (MetaLearn 2020)*. NeurIPS, 2020.
- [54] Xinyue Zhuang, Yu Cheng, Zhe Gan, Jingjing Liu, Lichao Liu, Guangsen Chen, Haoxuan Zhang, Meng Wang, Shuohang Liu, and Jianfeng Gao. DyLoRA: Parameter-efficient tuning of pre-trained models via dynamic low-rank adaptation. In *Proceedings of the Association for Computational Linguistics (ACL)*, pages 2345–2356, 2023.
- [55] Yingtian Zou, Fusheng Liu, and Qianxiao Li. Unraveling model-agnostic meta-learning via the adaptation learning rate. In *International Conference on Learning Representations (ICLR)*. OpenReview.net, 2022.

A Theorem 1 and Proof

Readers can refer to the derivation process of DDPM [34] to understand the following derivation. To align with the subscript ordering of weights $\theta_0 \rightarrow \theta_M$, we reverse the index order of diffusion states x_i mentioned in [20, 34].

Theorem 1. *Given the number of diffusion steps T , an increasing noise schedule $\{\alpha_0, \dots, \alpha_T\}$, local target weights $\{\theta_d, \dots, \theta_{k*d}\}$, and let the inference process align with the vanilla diffusion algorithm, i.e.,*

$$x_{t+1} = \frac{1}{\sqrt{\bar{\alpha}_{t+1}}} \left(x_t - \sqrt{1 - \bar{\alpha}_{t+1}} \epsilon_\theta(x_t, t) \right). \quad (1)$$

*Then, the denoiser ϵ_ϕ can recover the target sequence $\{\theta_d, \dots, \theta_{k*d=M}\}$ from standard Gaussian noise x_0 with evenly T/k steps intervals, when ϵ_ϕ is trained by local consistency loss L^{loc} as follows:*

$$\begin{aligned} L^{loc} &= \underset{i \in (0, k]}{E} L_i^{loc}, \\ L_i^{loc} &= \underset{t \in [0, i*T/k]}{E} \left\| \sqrt{1 - \bar{\alpha}_t^i} \epsilon_\phi(x_t, t) - \sqrt{1 - \bar{\alpha}_t} \epsilon \right\|^2, \\ x_t &= \sqrt{\bar{\alpha}_t^i} \theta_{i*d} + \sqrt{1 - \bar{\alpha}_t^i} \epsilon, \end{aligned} \quad (2)$$

where $\bar{\alpha}_t = \prod_{j=t}^{T-1} \alpha_j$, $\bar{\alpha}_t^i = \prod_{j=t}^{i*T/k-1} \alpha_j$, and ϵ denotes standard Gaussian noise.

Proof. First, consider a single local target $\theta_{i*d=i*M/k} = x_{i*T/k}$, its inference chain $\{x_0, \dots, x_{i*T/k}\}$ and its increasing schedule $\{\alpha_0, \dots, \alpha_{i*T/k}\}$. Let $x_{i*T/k}$ be $x_{T'}$ and diffusion steps be $i*T/K$.

According to vanilla diffusion model, to maximize the likelihood $p(x'_T)$ of observed data x'_T , we need to minimize denoising matching term

$$\underset{t \in [0, T'), q(x_t | x_{T'})}{E} \left[D_{KL} (q(x_{t+1} | x_t, x'_T) \parallel p_\phi(x_{t+1} | x_t)) \right]. \quad (3)$$

In the KL divergence bracket, the left term can be expanded by the Bayesian Theorem. The right term is the inference process to be modeled with ϕ , whose expectation is given by Equation 1.

According to Bayes Theorem,

$$q(x_{t+1} | x_t, x_{T'}) = \frac{q(x_t | x_{t+1}, x_{T'}) q(x_{t+1} | x_{T'})}{q(x_{t+1} | x_{T'})}. \quad (4)$$

According to the Markov Rule and standard diffusion process,

$$\begin{aligned} q(x_t | x_{t+1}, x_{T'}) &= q(x_t | x_{t+1}) \\ &\sim \mathcal{N}(x_t; \sqrt{\alpha_t} x_{t+1} + \sqrt{1 - \alpha_t} \mathbf{I}). \end{aligned} \quad (5)$$

Recursively using the diffusion process on $\{x_{T'}, \dots, x_{t+1}\}$, we have

$$q(x_t | x_{T'}) \sim \mathcal{N}(x_t; \sqrt{\bar{\alpha}_t^{T'}} x_{T'}, (1 - \bar{\alpha}_t^{T'}) \mathbf{I}), \quad (6)$$

where $\bar{\alpha}_t^{T'} = \prod_{j=t}^{T'-1} \alpha_j$. Note that the coefficients here differ from those in the vanilla diffusion algorithm.

According to Equation 6, $q(x_{t+1} | x_{T'})$ can be written as

$$q(x_{t+1} | x_{T'}) \sim \mathcal{N}(x_{t+1}; \sqrt{\bar{\alpha}_{t+1}^{T'}} x_{T'}, (1 - \bar{\alpha}_{t+1}^{T'}) \mathbf{I}). \quad (7)$$

According to Equation 5 6 7, Equation 4 can be written as

$$\begin{aligned}
q(x_{t+1} | x_t, x_{T'}) &= \frac{q(x_t | x_{t+1}, x_{T'}) q(x_{t+1} | x_{T'})}{q(x_t | x_{T'})} \\
&\sim \frac{\mathcal{N}(x_t; \sqrt{\alpha_t} x_{t+1}, (1 - \alpha_t) \mathbf{I}) \mathcal{N}(x_{t+1}; \sqrt{\bar{\alpha}_{t+1}^{T'}} x_{T'}, (1 - \bar{\alpha}_{t+1}^{T'}) \mathbf{I})}{\mathcal{N}(x_t; \sqrt{\bar{\alpha}_t^{T'}} x_{T'}, (1 - \bar{\alpha}_t^{T'}) \mathbf{I})} \\
&\propto \exp \left\{ -\frac{1}{2} \left(\frac{1}{\frac{(1-\alpha_t)(1-\bar{\alpha}_{t+1}^{T'})}{1-\bar{\alpha}_t^{T'}}} \right) \left[x_{t+1}^2 - 2 \frac{\sqrt{\alpha_t} (1 - \bar{\alpha}_{t+1}^{T'}) x_t + \sqrt{\bar{\alpha}_{t+1}^{T'}} (1 - \alpha_t) x_{T'}}{1 - \bar{\alpha}_t^{T'}} x_{t+1} \right] \right\}.
\end{aligned}$$

According to the definition of Gaussian distribution, the variance of Equation 4 can be written as

$$\sigma_q(t) \propto \frac{(1 - \alpha_t)(1 - \bar{\alpha}_{t+1}^{T'})}{1 - \bar{\alpha}_t^{T'}} \mathbf{I},$$

the expectation can be written as

$$\mu(x_t, x_{T'}) \propto \frac{\sqrt{\alpha_t} (1 - \bar{\alpha}_{t+1}^{T'}) x_t + \sqrt{\bar{\alpha}_{t+1}^{T'}} (1 - \alpha_t) x_{T'}}{1 - \bar{\alpha}_t^{T'}}. \quad (8)$$

Recursively apply the reparameterization trick to Equation 5 in an iterative manner, we have:⁴

$$x_t = \sqrt{\bar{\alpha}_t^{T'}} x_{T'} + \sqrt{1 - \bar{\alpha}_t^{T'}} \epsilon. \quad (9)$$

Reorganize Equation 9, we have

$$x_{T'} = \frac{1}{\sqrt{\bar{\alpha}_t^{T'}}} (x_t - \sqrt{1 - \bar{\alpha}_t^{T'}} \epsilon).$$

Substitute $x_{T'}$ into Equation 8, we have

$$\begin{aligned}
\mu(x_t, x_{T'}) &\propto \frac{\sqrt{\alpha_t} (1 - \bar{\alpha}_{t+1}^{T'}) x_t + \sqrt{\bar{\alpha}_{t+1}^{T'}} (1 - \alpha_t) \frac{1}{\sqrt{\bar{\alpha}_t^{T'}}} (x_t - \sqrt{1 - \bar{\alpha}_t^{T'}} \epsilon)}{1 - \bar{\alpha}_t^{T'}} \\
&= \frac{1}{\sqrt{\alpha_t}} x_t - \frac{1 - \alpha_t}{\sqrt{1 - \bar{\alpha}_t^{T'}} \sqrt{\alpha_t}} \epsilon.
\end{aligned} \quad (10)$$

Returning to Equation 3, minimizing KL divergence is equivalent to minimizing the difference between the expectations of the two terms in the bracket. Equation 1 gives the expectation of the right term, i.e.,

$$x_{t+1} = \frac{1}{\sqrt{\alpha_t}} x_t - \frac{1 - \alpha_t}{\sqrt{1 - \bar{\alpha}_t} \sqrt{\alpha_t}} \epsilon_\phi,$$

where $\bar{\alpha}_t = \prod_{j=t}^{T-1} \alpha_j$.

⁴This step is relatively complex; it is recommended to refer to [34].

Equation 10 is the expectation of the left term. As a result, Equation 3 can be simplified to the form of the left-term' expectation minus the right-term's expectation:

$$\begin{aligned}
L_{T'} &= \underset{t \in [0, T']}{E} \|\mu(x_t, x_{T'}) - \mu_\phi(x_t, t)\|^2 \\
&= \underset{t \in [0, T']}{E} \frac{(1 - \alpha_t)^2}{\alpha_t(1 - \bar{\alpha}_t^{T'})(1 - \bar{\alpha}_t)} \|\sqrt{1 - \bar{\alpha}_t^{T'}} \epsilon_\phi - \sqrt{1 - \bar{\alpha}_t} \epsilon_{T'}\|^2 \\
&\propto \underset{t \in [0, T']}{E} \|\sqrt{1 - \bar{\alpha}_t^{T'}} \epsilon_\phi - \sqrt{1 - \bar{\alpha}_t} \epsilon\|^2.
\end{aligned} \tag{11}$$

Note that $\bar{\alpha}_t^{T'} = \prod_{j=t}^{T'-1} \alpha_j = \prod_{j=t}^{i*T/k-1} \alpha_j = \bar{\alpha}_t^i$. So we substitute $T' = i*T/k$ into to Equation 11, it yield:

$$\underset{t \in [0, i*T/k]}{E} \|\sqrt{1 - \bar{\alpha}_t^i} \epsilon_\phi(x_t, t) - \sqrt{1 - \bar{\alpha}_t} \epsilon\|^2$$

which is consistent with the intended formulation L_i^{loc} in Equation 2.

This means that L_i^{loc} enables the diffusion model to generate the inference chain from Gaussian noise to $\theta_{i*d} = \theta_{i*T/k}$ in $i*T/k$ steps.

Moreover, since the inference process is fixed, i.e., Equation. 1, $L^{loc} = \underset{i \in (0, k]}{E} L_i^{loc}$ allows any θ_{i*d} and $\theta_{(i+1)*d}$ to share the same inference chain. Their interval is

$$(i + 1) * T/k - i * T/k = T/k.$$

Thus, the proof is complete. □

B Proposition 1 and Proof

Proposition 1. *When $k = 1$, local consistency diffusion is equivalent to the vanilla diffusion algorithm.*

Proof. When $k = 1$, $d = M/k = M$, so $i \in (0, k] \rightarrow i = 1$. At this point, only the optimal weight $\theta_{i,d=M}$ is modeled.

Moreover, for $k = 1$, we have

$$\bar{\alpha}_t^i = \prod_{j=t}^{i*T/k-1} \alpha_j = \prod_{j=t}^{T-1} \alpha_j = \bar{\alpha}_t,$$

hence the two coefficients in Equation 2 are identical and can be simplified, making L_i equivalent to L_i^{loc} . This makes local consistency diffusion be equivalent to the vanilla diffusion algorithm. \square

C Theorem 2 and Proof

Lemma 1. Assume that the loss function $L^D(\cdot)$ is l -smooth and satisfies μ -strongly convex. Then, the sequence $\{\theta_i\}_{i=0}^M$ generated by the gradient descent update with step size $\frac{1}{l}$ satisfies

$$\|\theta_M - \theta_*\|^2 \leq \frac{2[L^D(\theta_0) - L^D(\theta_*)]}{\mu} \left(1 - \frac{\mu}{l}\right)^M.$$

Proof. Since $L^D(\theta)$ is l -smooth, for any θ and θ' ,

$$L^D(\theta') \leq L^D(\theta) + \nabla L^D(\theta)^\top (\theta' - \theta) + \frac{l}{2} \|\theta' - \theta\|^2.$$

Applying this to the gradient descent update $\theta_{k+1} = \theta_k - \frac{1}{l} \nabla L^D(\theta_k)$, we have

$$\begin{aligned} L^D(\theta_{k+1}) &\leq L^D(\theta_k) + \nabla L^D(\theta_k)^\top (\theta_{k+1} - \theta_k) + \frac{l}{2} \|\theta_{k+1} - \theta_k\|^2 \\ &= L^D(\theta_k) - \frac{1}{2l} \|\nabla L^D(\theta_k)\|^2. \end{aligned} \tag{12}$$

Since $L^D(\theta)$ is μ -strongly convex, it satisfies the Polyak–Lojasiewicz condition:

$$\frac{1}{2} \|\nabla L^D(\theta)\|^2 \geq \mu [L^D(\theta) - L^D(\theta_*)].$$

Substituting this inequality into Equation 12, we have

$$L^D(\theta_{k+1}) \leq L^D(\theta_k) - \frac{\mu}{l} (L^D(\theta_k) - L^D(\theta_*)).$$

The above equation can be reorganized to

$$L^D(\theta_{k+1}) - L^D(\theta_*) \leq \left(1 - \frac{\mu}{l}\right) (L^D(\theta_k) - L^D(\theta_*)).$$

Start from $k = 0$, and recursively apply the above equation with M times. It follows that

$$L^D(\theta_M) - L^D(\theta_*) \leq \left(1 - \frac{\mu}{l}\right)^M (L^D(\theta_0) - L^D(\theta_*)).$$

Since $L^D(\theta)$ is μ -strongly convex, it satisfies

$$\|\theta - \theta_*\|^2 \leq \frac{2}{\mu} (L^D(\theta) - L^D(\theta_*)).$$

So we have

$$\begin{aligned} \|\theta_M - \theta_*\|^2 &\leq \frac{2}{\mu} (L^D(\theta_M) - L^D(\theta_*)) \\ &\leq \frac{2(L^D(\theta_0) - L^D(\theta_*))}{\mu} \left(1 - \frac{\mu}{l}\right)^M. \end{aligned}$$

□

Theorem 2. Assume that the reconstruction error of the generative model is bounded by c , the downstream loss is bounded by ψ , and the loss function is both l -smooth and μ -strongly convex, with the eigenvalues of the Hessian matrix around the optimum θ_* bounded by λ . Then, the cumulative empirical error of the weight generation paradigm can be bounded as follows:

$$L^D(\hat{\theta}) - L^D(\theta_*) \leq \frac{\lambda}{2} \left[c + \frac{2\psi}{\mu} \left(1 - \frac{\mu}{l}\right)^M \right], \quad (13)$$

where $\hat{\theta}$ is the weight predicted by the generative model.

Proof. Using the Taylor expansion around the optimal point θ_* , we have

$$\begin{aligned} L^D(\hat{\theta}) - L^D(\theta_*) &= \nabla L^D(\theta_*)^T (\hat{\theta} - \theta_*) + \frac{1}{2} (\hat{\theta} - \theta_*)^T \nabla^2 L^D(\xi) (\hat{\theta} - \theta_*) \\ &= \frac{1}{2} (\hat{\theta} - \theta_*)^T \nabla^2 L^D(\xi) (\hat{\theta} - \theta_*). \end{aligned} \quad (14)$$

According to a constraint on the Hessian matrix, we have

$$\frac{1}{2} (\hat{\theta} - \theta_*)^T \nabla^2 L^D(\xi) (\hat{\theta} - \theta_*) \leq \frac{\lambda}{2} \|\hat{\theta} - \theta_*\|^2. \quad (15)$$

Decomposing $\|\hat{\theta} - \theta_*\|^2$ into weight preparation error and reconstruction error, we have

$$\begin{aligned} \|\hat{\theta} - \theta_*\|^2 &\leq \|\hat{\theta} - \theta_M\|^2 + \|\theta_M - \theta_*\|^2 \\ &\leq c + \frac{2(L^D(\theta_0) - L^D(\theta_*))}{\mu} \left(1 - \frac{\mu}{l}\right)^M \text{ (Using Lemma 1)} \\ &\leq c + \frac{2\psi}{\mu} \left(1 - \frac{\mu}{l}\right)^M. \end{aligned} \quad (16)$$

Substituting Equation 16 and Equation 15 into Equation 14 we obtain

$$L^D(\hat{\theta}) - L^D(\theta_*) \leq \frac{\lambda}{2} \left[c + \frac{2\psi}{\mu} \left(1 - \frac{\mu}{l}\right)^M \right].$$

□

D Preliminary

D.1 Diffusion Model

The core idea of the diffusion model is to model data through a two-stage process:

- **Diffusion Process:** Starting with data x_T , noise is added at each step to generate x_0 , eventually approaching a standard normal distribution.
- **Inference Process:** Starting with noise x_0 , a denoising model ϕ generates x_1, x_2, \dots, x_T step by step.

By precisely modeling the reverse process, the diffusion model ϕ can generate new samples that match the original data distribution. Diffusion models define an increasing schedule $\{\alpha_i\}_{i=0}^T$ to control the noise level at each step. In the diffusion process, noise is added at each step t , transforming the data x_{t+1} into x_t

$$q(x_t|x_{t+1}) = \mathcal{N}(x_t; \sqrt{\alpha_t}x_{t+1}, (1 - \alpha_t)\mathbf{I}).$$

The direct transition from x_T to x_t can be written as

$$q(x_t|x_T) = \mathcal{N}(x_t; \sqrt{\bar{\alpha}_t}x_T, (1 - \bar{\alpha}_t)\mathbf{I}),$$

where $\bar{\alpha}_t = \prod_{i=t}^{T-1} \alpha_i$ is the cumulative noise schedule, controlling the overall noise level from x_0 to x_t . In the inference process, the denoiser iteratively reconstructs the data by

$$x_{t+1} = \frac{1}{\sqrt{\alpha_t}}x_t - \frac{1 - \alpha_t}{\sqrt{1 - \bar{\alpha}_t}\sqrt{\alpha_t}}\epsilon_\phi + \sigma_z\epsilon,$$

We omit the additional $\sigma_z\epsilon$ for stable weight generation. The key point of training a variational model is to maximize the Evidence Lower Bound (ELBO). In the diffusion algorithm, optimizing the ELBO is essentially equivalent to minimizing the denoising match term

$$\mathbb{E}_{t \in [0, T'], q(x_t|x_{T'})} [\text{D}_{\text{KL}}(q(x_{t+1}|x_t, x'_T) \parallel p_\phi(x_{t+1}|x_t))].$$

which is also the objective optimized by our local consistency diffusion.

D.2 REPTILE

REPTILE is a first-order optimization-based meta-learning algorithm that simplifies training while retaining strong adaptability across tasks. It eliminates the need for second-order gradients, making it computationally efficient compared to algorithms like MAML. The training process consists of two loops: the inner-loop and the outer-loop.

In the inner loop, REPTILE performs gradient descent on a sampled task T_i using the task's support set. Starting from the meta-parameters ϕ , the task-specific parameters ϕ_i are updated for K steps using

$$\phi_i^{(t+1)} = \phi_i^{(t)} - \eta \nabla_{\phi_i^{(t)}} L_{T_i}(\phi_i^{(t)}),$$

where η is the inner-loop learning rate and L_{T_i} is the loss for the task T_i .

In the outer-loop, the meta-parameters ϕ are updated by moving them toward the task-specific parameters ϕ_i obtained from the inner loop. This meta-update is given by

$$\phi \leftarrow \phi + \zeta(\phi_i - \phi),$$

where ζ is the outer-loop learning rate.

By iteratively repeating the inner and outer loops across multiple tasks drawn from the task distribution \mathcal{T} , REPTILE optimizes the meta-parameters ϕ to find an initialization that enables fast adaptation to new tasks with minimal gradient steps. Its simplicity lies in avoiding second-order derivatives, while its effectiveness is demonstrated across diverse applications such as few-shot learning and domain generalization.

E Setup Details

E.1 Dataset

Omniglot. The raw Omniglot dataset contains 1623 handwritten characters from 50 alphabets, each with 20 instances in 28×28 grayscale format. We partition the classes of the training set, evaluation set, and testing set into 800:400:432. We use Omniglot in three scenarios. We used the Omniglot dataset in our preliminary experiments, ablation experiments, and comparative experiments. For the construction of the classification task, we referred to the experimental setup by MAML.

Mini-ImageNet. The raw Mini-ImageNet contains 100 classes, each containing 600 instances in 84×84 grayscale format. We partition classes of training set, evaluation set, and testing set into 64:16:20. The usage of Mini-ImageNet is the same as Omniglot, and we also follow the setup given by MAML.

Tiered-ImageNet. The Tiered-Imagenet dataset is a larger-scale few-shot learning benchmark derived from ImageNet, containing 608 classes grouped into 34 higher-level categories. Each image is in 84×84 resolution with RGB channels. Following the standard protocol (Meta-Baseline), we partition the dataset into 351 classes for training, 97 for validation, and 160 for testing, ensuring no class overlap across phases. We use Tiered-ImageNet in all experimental stages, including ablation and comparative evaluations, to assess the generalization ability of our method on a more diverse and semantically structured dataset.

ImageNet-1K. The raw ImageNet-1K is a benchmark dataset with 1000 classes, 1.2 million training images, and 50000 validation images, typically resized to a resolution of 224×224 pixels. We partitioned the dataset into 20k subsets, each containing 50 classes with 50 images per class. We use this dataset for pre-training and perform transfer learning evaluation on other unseen datasets.

CIFAR-10 CIFAR-100 STL-10 Aircraft Pets. CIFAR-10 and CIFAR-100 are image datasets introduced by Alex Krizhevsky, containing 60000 images resized to 32×32 pixels. CIFAR-10 includes 10 classes, while CIFAR-100 features 100 fine-grained classes. STL-10, derived from ImageNet, consists of 10 classes with 13000 labeled images and 100000 unlabeled images, with a resolution of 96×96 pixels. The Aircraft dataset includes 10000 images across 100 aircraft models, with hierarchical labels for manufacturer, family, and variant. The Pets dataset consists of 7349 images of 37 pet breeds, with annotations for class labels, bounding boxes, and pixel-level segmentation. We use these datasets to evaluate the model’s transfer learning capabilities, which means the labels of these datasets are not visible to the model.

DomainNet. DomainNet is a dataset for multi-domain generalization. We use it to evaluate algorithms’ ability for few-shot domain generalization. It consists of 345 classes from 6 domains, with a resolution of 224×224 pixels. We use Clipart, Infograph, Painting, Quickdraw, and Real domains for training, while Sketch domains are for testing. The tasks we constructed are 5-way 1-shot and 20-way 5-shot. Note that the testing set shares the same 345 classes as the training set.

GLUE. The GLUE Benchmark (General Language Understanding Evaluation) tests models on 9 diverse NLP tasks, including CoLA for grammatical acceptability, SST-2 for sentiment classification, MRPC for paraphrase detection, STS-B for sentence similarity, QQP for duplicate question detection, MNLI for natural language inference, QNLI for question-answer validation, RTE for entailment

classification, and WNLI for pronoun resolution. We use this dataset to test the efficiency of different algorithms for multi-task fine-tuning on LLM models. Specifically, we use five binary classification tasks, i.e., SST-2, QQP, RTE, WNLI, and CoLA for the training of Mc-Di. Then we use the other two tasks, i.e., MRPC and QNLI, to evaluate the performance of different fine-tuning algorithms.

E.2 Model Configuration

For the downstream network θ , we adopt different architectures for different tasks. In tasks on the Omniglot and Mini-ImageNet datasets, we follow the standard setup used by most meta-learning methods, employing 4 convolution blocks with batch normalization and ReLU with a linear probe for classification. For zero-shot tasks on CIFAR-10, CIFAR-100, STL-10, Aircraft, and Pets, we use the commonly adopted ResNet-12 with a linear probe for classification. In multi-domain generalization tasks, we maintain the same setup with [17]. In the LLM multi-task fine-tuning scenario, the downstream network is the LLM model itself, i.e., RoBERTa-base. For the diffusion model f_ϕ^G , Mc-Di employs the same U-Net architecture given by Meta-Diff [50]. The task embedding Emb_{T_i} is calculated by a ResNet101 backbone used by [5]. In the weight preparation stage, the real-world optimizer (Adam) uses a fixed learning rate of 0.005 and an automatic early-stopping strategy [43] to determine the downstream task training epoch M . In the meta-training stage, we set the learning rate η , meta-learning rate ζ and training epochs to 0.005, 0.001, and 6000, respectively. The segment number k is set to 3, and the diffusion step T is set to 20.

F Additional Experiments

F.1 Sensitive Study

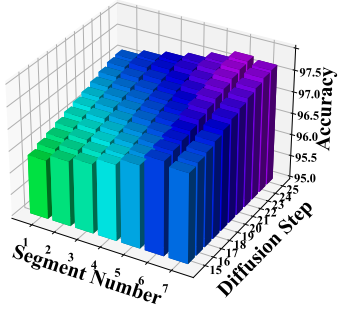


Figure 8: Sensitive study on Omniglot

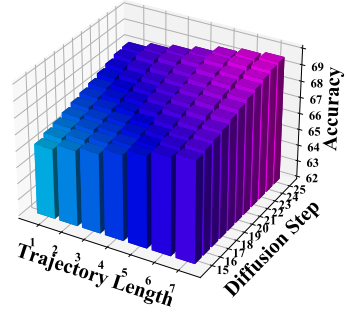


Figure 9: Sensitive study on Mini-Imagenet

Compared to existing weight generation methods, the two hyperparameters of Mc-Di, i.e., segment number and diffusion steps, may affect the model’s sensitivity. To evaluate the robustness of our approach, we analyze the impact of segment number and diffusion steps on classification accuracy for Mini-ImageNet and Omniglot. As shown in Figure 8 and Figure 9, the accuracy remains stable across different parameter settings, with only minor variations. While increasing segment number and diffusion steps can slightly improve performance, excessive changes do not lead to significant degradation. The consistency across both datasets indicates that Mc-Di is insensitive to these hyperparameters, demonstrating robustness. Note that we do not use the parameter combination that achieves the highest accuracy in this experiment as the default setting. We aim to maintain performance above the state-of-the-art levels while reducing computational costs during inference.

F.2 Adaptability to Different Architectures

To verify the effectiveness of Mc-Di under different scale network structures, we compare them with their degraded versions, i.e., REPTILE, TW-Di, and Mv-Di. Table 6 and Table 7 show the effectiveness of our method on Swin Transformer, ResNet18, and MobileNetV2 architectures. The results demonstrate that each component of our method remains effective across neural network architectures of different scales.

Method	Swin Transformer	ResNet18	MobileNetV2
REPTILE	98.27	97.11	93.79
TW-Di	97.43	96.60	93.61
Mv-Di	98.93	98.44	94.92
Mc-Di	99.90	98.82	95.84

Table 6: Comparison of accuracy across different network structures on Omniglot 5-way 1-shot tasks.

Method	Swin Transformer	ResNet18	MobileNetV2
REPTILE	57.27	52.55	40.67
TW-Di	66.26	60.32	53.27
Mv-Di	76.75	70.76	59.33
Mc-Di	82.38	77.85	64.81

Table 7: Comparison of accuracy across different network structures on Mini-ImageNet 5-way 1-shot tasks.

F.3 Domain Generalization

We added the 5-way 1-shot domain generalization experiment on Meta-Dataset [48] in Table 8.

Method	Traffic Sign	MSCOCO	MNIST	CIFAR-100	CIFAR-10	Avg	Latency (ms)
REPTILE	43.32 ± 0.88	39.62 ± 1.02	68.50 ± 0.88	40.60 ± 0.98	43.73 ± 0.94	47.15	26.8
Meta-Baseline	47.52 ± 0.92	41.20 ± 1.04	68.47 ± 0.85	43.07 ± 0.85	46.02 ± 0.90	49.26	26.2
Meta-Hypernetwork	55.91 ± 0.91	48.47 ± 0.91	80.55 ± 0.91	50.67 ± 0.91	54.14 ± 0.91	57.95	10.3
GHN3	44.22 ± 0.93	47.27 ± 1.14	76.44 ± 0.91	36.38 ± 0.83	42.52 ± 1.06	49.37	20.1
OCD	52.14 ± 0.90	57.74 ± 1.12	75.23 ± 0.92	47.51 ± 0.91	55.54 ± 1.13	57.63	9.7
Meta-Diff	57.19 ± 0.94	60.01 ± 1.04	78.47 ± 0.94	55.29 ± 0.89	61.38 ± 1.01	62.47	10.9
Mv-Di (ours)	58.48 ± 1.02	60.58 ± 1.00	80.82 ± 0.93	55.13 ± 0.93	62.93 ± 1.04	63.59	7.0
Mc-Di (ours)	59.46 ± 0.99	62.70 ± 1.01	83.65 ± 0.94	57.07 ± 0.91	65.11 ± 1.05	65.60	5.2

Table 8: Comparison of 5-way 1-shot performance on the last 5 unseen datasets of Meta-Dataset. These methods are trained on the first 8 datasets of Meta-Dataset.

G Related Work

Meta-Learning. Meta-learning often employs a bi-level optimization-based paradigm [12, 44, 4, 13, 11] for better generalization performance [25, 24, 3, 16, 2] on few-shot and reinforcement learning tasks. However, it incurs significant costs for weight fine-tuning, especially in multi-task scenarios. Methods like ANIL [44] and Reptile [39] improve training efficiency by minimizing updates to only essential task-specific layers or by approximating meta-gradients, respectively. However, these methods still rely on gradient computation and fail to achieve superior accuracy.

Network Weights Generation. Hypernetwork [18] is the first method that uses one network to generate another’s weights, leading to extensions like the HyperSeg [40] for downstream task flexibility. Conditional diffusion models provide another approach [10], with OCD leveraging overfitting [35] and Meta-Diff enhancing few-shot adaptability [50]. Hyper-representations [46] embed model characteristics to support weight generation for unseen tasks, while Image-free Classifier Injection [5] achieves zero-shot classification via semantic-driven weights. These methods are constrained by their single-level optimization approach, which presents limitations in both cross-task knowledge transfer capabilities and potential adaptability to new tasks. Note that Meta-Diff essentially uses a single-level optimization strategy (see its Algorithm.1 for evidence). Most importantly, these methods overlook the supervision signal in local target weights, limiting the model’s efficiency and accuracy.